IV International Conference on Computational Methods for Coupled Problems in Science and Engineering
COUPLED PROBLEMS 2011
M. Papadrakakis, E. Oñate and B. Schrefler (Eds)

APPLICATION OF A VISCOPLASTIC DAMAGE MODEL FOR THE FAILURE PREDICTION OF REGENERATIVELY COOLED NOZZLE STRUCTURES

VIVIAN TINI*, IVAYLO N. VLADIMIROV AND STEFANIE REESE

*Institute of Applied Mechanics
RWTH Aachen University
Mies-van-der-Rohe Straße, 52074 Aachen, Germany
e-mail: vivian.tini@rwth-aachen.de, www.ifam.rwth-aachen.de

Key words: Regeneratively Cooled Noozle, Combustion Chamber, Dog-house Effect, Lifetime Prediction, Viscoplastic-Damage Model, Thermomechanical Analysis

Abstract. Regeneratively cooled nozzle structures belong to the critical components of a space shuttle main engine. The cooling channel wall in the combustion chamber is subjected to extreme cyclic thermomechanical loadings which eventually lead to the damage of the wall, well known as the "dog-house" effect. A material model for the purpose of reliable lifetime prediction is being developed. The model shall describe the material behaviour under hardening conditions as well as the superimposed effect of fatigue which occurs due to cyclic loadings.

Motivated by extending the classical rheological model for elastoplasticity with Armstrong-Frederick kinematic hardening, a viscoplastic model is formulated in the small strain regime. The coupling with damage is performed using the well-known concept of effective stress and the principle of strain equivalence. Parameter identification on the basis of experimental results for the high temperature copper alloy NARloy-Z, which is one of the typical cooling channel liner materials, is performed. The applicability of the model will be shown by means of sequentially coupled thermomechanical analyses.

1 INTRODUCTION

The regeneratively cooled rocket thrust chamber is one of the most critical components determining the performance of a Reusable Launch Vehicle (RLV). Over the years research in the field of structural computation has been performed with the goal to optimize the overall performance of rocket engines.

Finite element analyses have been implemented to simulate the cooling channel response under in-service conditions [1-8]. These previous studies mainly focused on the

application of a viscoplastic material model to describe the dog-house failure mode [1, 2, 8], as well as important factors influencing the lifetime of the combustion chamber wall [3, 5]. With the exception of the work of Schwarz et al. [8], only 2D structural analyses were performed and the material modelling did not include the effect of damage. The work of Schwarz incorporates aging as well as the crack closure effect to describe the dog-house effect.

Failure prediction of the thrust chamber structure requires complete description of the cooling channel response under extreme operating conditions. There are many factors to be considered such as the chemical reactions during the combustion process, the fluid flow in the thrust chamber and the cooling channels and the heat transfer between the fluid flow and the chamber wall structure. This makes up a complex system. For reliable lifetime prediction purposes fluid-structure-interaction analyses are indeed required.

This paper will focus on the application of a viscoplastic damage model in structural thermomechanical analyses. The thermal loads are applied in a heat transfer analysis to obtain the temperature field history of the combustion chamber segment. The temperature history is then given as input for subsequent structural analyses, where the cyclic evolution of damage is to be seen.

In the following sections the development of the model based on the well known rheological model of Armstrong-Frederick kinematic hardening will be elaborated. The material parameters are obtained by fitting tensile test experimental data performed for NARloy-Z copper alloy. Finally results of the implementation of the viscoplastic damage model for the thermomechanical analyses will be shown.

2 THE VISCOPLASTIC DAMAGE MODEL

2.1 Continuum mechanical approach by a rheological model

First of all, we extend the classical rheological model for elastoplasticity with Armstrong-Frederick kinematic hardening shown in Fig. 1(a) to include rate-dependent effects. This is done by adding a dashpot element with the viscosity parameter η as shown in Fig. 1(b). In the small strain regime, both models employ an additive decomposition of the total strain ε into elastic and inelastic parts, i.e. $\varepsilon = \varepsilon_e + \varepsilon_p$ and $\varepsilon_p = \varepsilon_{pe} + \varepsilon_{pi}$.

The spring stiffness constants are represented by the parameters E and E_h. The serially connected dashpot in Fig. 1(a) with the "pseudo"-viscosity parameter $\eta_h = E_h/(\dot{\lambda}b)$ is not a dashpot in the true sense, however by choosing the right value of the spring constant E_h and the dimensionless parameter b, the nonlinear effect of kinematic hardening can be represented. Here $\dot{\lambda}$ is the plastic multiplier.

Coupling with damage is shown schematically in Fig. 1(b) using dotted lines for the elastic spring. The spring constant E_d is defined as

$$E_d = E(1 - D) \tag{1}$$

where D is the scalar variable for isotropic damage (Kachanov 1958) [9]. The wellknown concept of effective stress (Rabotnov 1968)[9] is applied, therefore the effective stress takes

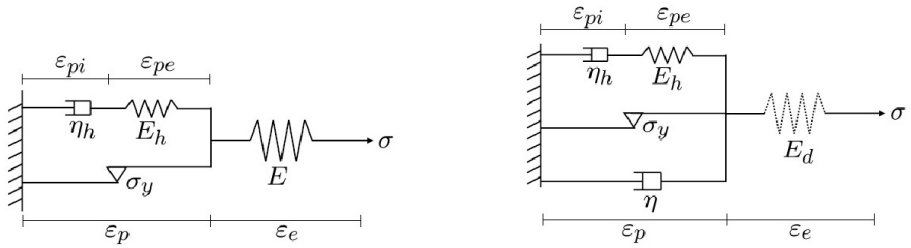

(a) Rheological model of Armstrong-Frederick kinematic hardening[10].

(b) Extension of the Armstrong-Frederick kinematic hardening model into a viscoplastic damage model.

Figure 1: The classical rheological model of Armstrong-Frederick kinematic hardening and its extension into a viscoplastic damage model.

the form

$$\tilde{\sigma} = \frac{\sigma}{(1-D)} \tag{2}$$

In this viscoplastic damage model $\dot{\lambda}$ is computed using the Perzyna formulation, $\dot{\lambda} = \langle \Phi \rangle / \eta$, where η is the viscosity parameter. The symbol $\langle \cdot \rangle$ defines the Macauley brackets i.e. $\langle x \rangle = \frac{x+|x|}{2}$.

2.2 Three dimensional extension within small strains formulation

Based on the rheological model and the principle of strain equivalence, the constitutive equations are generalized for three dimensions. Assuming elastic isotropic response, the stress-strain relationship can be written as $\boldsymbol{\sigma} = \widetilde{\mathbf{C}}_1 [\boldsymbol{\varepsilon} - \boldsymbol{\varepsilon}_p]$, $\widetilde{\mathbf{C}}_1 = (1-D)\,\mathbf{C}_1$, where $\mathbf{C}_1$ is the fourth order elasticity tensor. The back stress tensor is defined as $\boldsymbol{X} = \mathbf{C}_2 [\boldsymbol{\varepsilon}_{pe}]$, where $\mathbf{C}_2$ is another elasticity tensor. The components of both elasticity tensors depend on the elastic moduli E_1, E_2 and the Poisson's ratios ν_1, ν_2, respectively.

Applying J_2 flow theory and nonlinear isotropic hardening, the loading function is taken from the von Mises condition:

$$\Phi = \left\| \widetilde{\boldsymbol{\sigma}}^D - \boldsymbol{X}^D \right\| - \sqrt{\frac{2}{3}} (\sigma_y + R) \tag{3}$$

where $(\cdot)^D$ represents the deviatoric term of the tensor. The isotropic hardening function is defined as

$$R = Q_0 (1 - \exp(-\kappa \alpha)) \tag{4}$$

where α is the internal variable for isotropic hardening, Q_0 and κ are material parameters. The evolution equations of the plastic strain $\boldsymbol{\varepsilon}_p$, the inelastic part of the plastic strain $\boldsymbol{\varepsilon}_{pi}$,

and the accumulated plastic strain α are given as follows:

$$\dot{\boldsymbol{\varepsilon}}_p = \frac{\dot{\lambda}}{1-D} \frac{\widetilde{\boldsymbol{\sigma}}^D - \boldsymbol{X}^D}{\left\| \widetilde{\boldsymbol{\sigma}}^D - \boldsymbol{X}^D \right\|}, \; \dot{\boldsymbol{\varepsilon}}_{pi} = \dot{\lambda}\, b\, \boldsymbol{\varepsilon}^D_{pe}, \; \dot{\alpha} = \sqrt{\frac{2}{3}}\, \dot{\lambda} \tag{5}$$

The isotropic damage variable D is assumed to evolve in the following way over time:

$$\dot{D} = \sqrt{\frac{2}{3}} \frac{\dot{\lambda}}{1-D} \left(\frac{Y}{S} \right)^k H_{(\alpha - p_D)}, \; Y = \frac{1}{2} \boldsymbol{\varepsilon}_e \cdot \mathbf{C}_1 \left[\boldsymbol{\varepsilon}_e \right] \tag{6}$$

Here p_D is the damage threshold and Y is the strain energy density release rate. The step function H is zero for $\alpha < p_D$ and is equal to one for $\alpha \geq p_D$. The rate of damage evolution is influenced by the material parameters S and k. The plastic multiplier is defined to take the form

$$\dot{\lambda} = \frac{\left\langle \overline{\Phi}^m \right\rangle}{\eta}, \; \overline{\Phi} = \frac{\left\| \widetilde{\boldsymbol{\sigma}}^D - \boldsymbol{X}^D \right\|}{\sqrt{\frac{2}{3}} \left(\sigma_y + R \right)} - 1 \tag{7}$$

where m is a material parameter. In total the model has 13 parameters: E_1, ν_1, E_2, ν_2, σ_y, Q_0, κ, b, S, k, p_D, η, m. The Poisson's ratios ν_1 and ν_2 are assumed to be constant with respect to temperature. Other parameters depend on temperature.

3 FITTING WITH EXPERIMENTAL DATA

Mechanical and physical properties of the NARloy-Z alloy, such as the modulus of elasticity, the Poisson's ratio, the density, specific heat, thermal conductivity, and the coefficient of thermal expansion are obtained from the experimental report of six candidate rocket materials prepared by Esposito et al. for the NASA Lewis Research Center [11]. The yield stress and the kinematic hardening parameters are defined by fitting the model response to tensile stress-strain curves at 27.6 K, 294.3 K, 533.1 K and 810.9 K. The temperature dependency of these parameters is defined to be linear.

For the material parameters and the model response see Table 3 and Fig. 3. The values of these parameters at other temperatures are obtained by linear interpolation. The experimental data are represented by different symbols (see "exp 27.6", "exp 294.3", "exp 593.1", "exp 810.9"). The simulation results are plotted as solid lines. It is assumed that damage has not taken place yet. Furthermore, viscous effects are neglected. The tensile tests were performed at a strain rate of 0.002 s^{-1}.

Identification of the damage parameters p_D, S, k and the parameters η and m requires tensile tests until rupture as well as relaxation tests at different temperatures. Unfortunately these data are barely available and experimental work is beyond the scope of the current project.

σ_y [MPa]	E_2 [GPa]	b [$-$]	θ [K]
190	7.47	155	27.6
158	7.84	150	294.3
130	7.49	170	533.1
90	7.71	225	810.9

Table 1: The value of the yield stress and the kinematic hardening parameters fitted at the test temperatures.

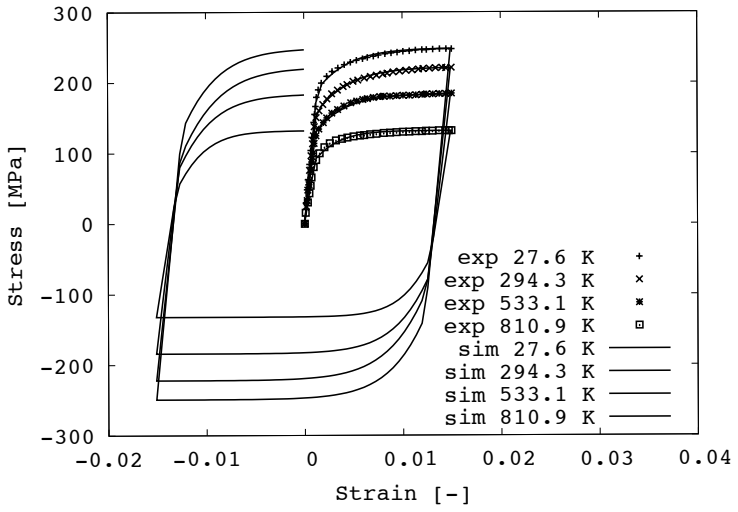

Figure 2: Tensile tests on NARloy-Z. Experimental results are taken from [11] and shown by the different symbols, computational results are shown by the solid lines.

4 THERMOMECHANICAL ANALYSES OF THE COMBUSTION CHAMBER SEGMENT

The viscoplastic damage model presented is discretized using the implicit backward Euler scheme and is implemented as a user subroutine UMAT into the Abaqus finite element analysis software. First of all, a transient thermal analysis of the combustion chamber segment is performed to obtain the temperature field of the entire chamber segment. The temperature history is then used as input for the user subroutine in the static analyses.

4.1 Transient thermal analysis

Fig. 3(a) shows the schematic cross section of a typical combustion chamber. The outer wall is made out of nickel alloy. The cooling channel walls are made out of copper alloy. The red and blue areas show where the hot gas and the coolant flow.

The geometry of the modelled segment is the quasi Vulcain geometry following the

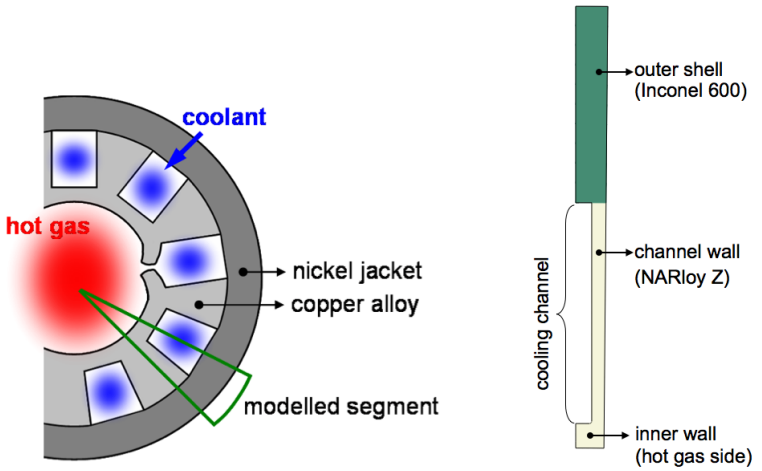

(a) Schematic cross section of a typical rocket combustion chamber.

(b) Modelled segment of the quasi Vulcain thrust chamber at the throat.

Figure 3: Schematic cross section of a combustion chamber and the modelled segment.

Phase	Time [s]	T_{hotgas} [K]	$T_{coolant}$ [K]
Pre-cooling	0 - 2	40	40
Hot run	3 - 603	950	40
Post-cooling	604 - 605	40	40
Relaxation	605 - 620	293.15	-

Table 2: Thermal cycle applied for the transient thermal analysis.

work of Kuhl et al. [12]. Convective thermal boundary conditions are employed at the inner and outer radii as well as in the cooling channel similar to the work of Riccius et al. [4]. The left and right sides have zero flux boundary conditions to ensure symmetry of the thermal field. The thermal cycle described in Table 2 is applied in the analysis. Fig. 4 shows some snapshots of the temperature field resulting from the transient thermal analysis.

4.2 Static analyses

The resulting temperature distribution from the thermal analysis is used as input for subsequent 3D static analyses. The goal of the static analysis is to see the feasibility of the implemented viscoplastic damage model to describe the dog-house failure mode qualitatively. The pressure cycle in Table 3 is applied as load in the static analyses.

For the static analyses 8-node brick elements with reduced integration were applied.

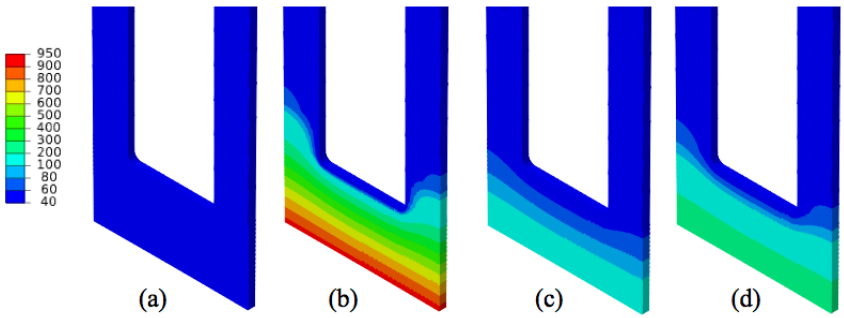

Figure 4: Temperature distribution of the combustion chamber segment at different phases of the assumed operational cycle: (a) pre cooling (b) hot run (c) post cooling (d) relaxation.

Phase	Time [s]	P_{hotgas} [MPa]	$P_{coolant}$ [MPa]
Pre-cooling	0 - 2	0	2
Hot run	3 - 603	10	14.5
Post-cooling	604 - 605	0	2
Relaxation	605 - 620	0	0

Table 3: Pressure cycle applied for the static analyses.

The critical area of interest is the cooling channel wall at the hot gas side. Two different meshes were used. The coarser and the finer mesh have in total 1338 and 4014 elements respectively. Fig. 5 shows the discretization of the hot gas side wall using both meshes. The corner of the cooling channel passage is rounded with 0.1 mm fillet radius.

The damage contours obtained from the analyses are shown in Fig. 6. The computation using Mesh 1 could be performed up to 16 cycles. Applying Mesh 2 the computation could be performed up to 13 cycles. As the damage increases, the local iteration within the user subroutine requires smaller and smaller time steps. The corresponding cyclic damage evolutions over time are shown in Fig. 7. Here it can be seen that with the coarser mesh, the damage evolves slightly faster, in comparison to the one obtained using the finer mesh. As mentioned before, the analyses were performed neglecting viscous effects. This might be the reason of the mesh dependency of the result. This phenomenon is well known to occur in elastoplasticity coupled with damage due to the change of the type of the differential equations to be solved as damage evolves.

Improvement on the robustness of the computation shall enable further computations, such that no convergence problem would occur as the number of elements with very low stiffness due to damage grows. Fig. 8(a) shows the predicted end shape of the cooling channel segment. The grey area represents the area mostly affected by damage. Fig. 8(b) shows the cross section of a combustion chamber made out of the NARloy-Z copper alloy. It is mentioned by Hannum et al. [13] that low cycle fatigue has stronger influence on the dog-house failure mode occuring within a NARloy-Z combustion chamber. It can be

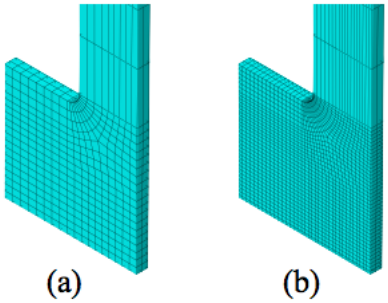

Figure 5: (a) Mesh 1 with 1338 elements (b) Mesh 2 with 4014 elements

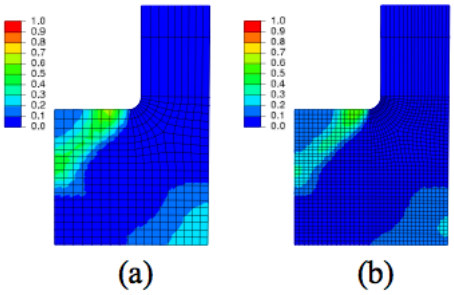

Figure 6: Damage contour obtained using the viscoplastic damage model implemented in UMAT: (a) Mesh 1 at the 16th cycle. (b) Mesh 2 at the 13th cycle.

seen that the hot gas side wall does not bulge so much towards the chamber. On the contrary, in an OFHC combustion chamber, it has been observed that the hot gas side wall becomes significantly thinner and bulges more towards the interior of the chamber. It is mentioned that crack occurs after the occurence of a necking phenomenon. For both materials, the typical dog-house shape of the cooling channels are to be seen. However depending on the liner material, the failure cause can be different.

5 CONCLUSIONS

In this work the application of a viscoplastic damage model for the failure prediction of a typical rocket combustion chamber wall made from NARloy-Z has been presented. Further improvement on the robustness of the computation, as well as considering temperature dependency of the damage and viscosity parameters shall enable better failure prediction.

6 ACKNOWLEDGEMENT

Financial support of the German Research Foundation (DFG) within the project CRC/Transregio 40 Fundamental Technologies for the Development of Future Space-

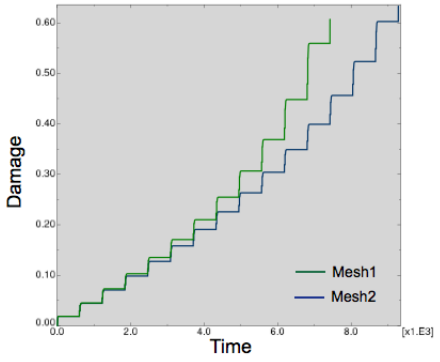

Figure 7: The cyclic evolution of the damage over time.

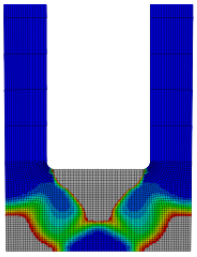

(a) Predicted end shape of the cooling channel segment.

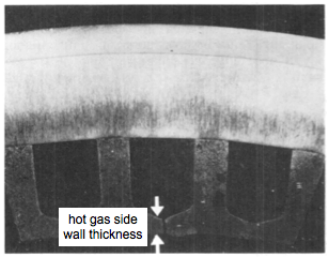

(b) The dog-house failure mode occured in a NARloy-Z thrust chamber. [13]

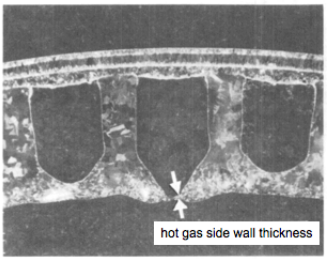

(c) The dog-house failure mode occured in an OFHC thrust chamber. [13]

Figure 8: The predicted end shape of the channel segment from the simulation and the dog-house failure mode.

Transport-System Components under High Thermal and Mechanical Loads is gratefully acknowledged.

REFERENCES

[1] Vinod K. Arya. Viscoplastic analysis of an experimental cylindrical thrust chamber liner. *AIAA Journal*, 30(3):781–789, March 1992.

[2] D.T. Butler. Jr, Jacob Aboudi, and Marek-Jerzy Pindera. Role of the material constitutive model in simulating the reusable launch vehicle thrust cell liner response. *Journal of Aerospace Engineering*, 18(1):28–41, 2005.

[3] Jörg R. Riccius, Malte R. Hilsenbeck, and Oskar J. Haidn. Optimization of geometric parameters of cryogenic liquid rocket combustion chambers. In *AIAA 2001-3408*, 1–11, AIAA, 2001.

[4] Jörg R. Riccius and E. B. Zametaev. Stationary and dynamic thermal analyses of cryogenic liquid rocket combustion chamber walls. In *38th AIAA/ASME/SAE/ASEE Joint Propulsion Conference and Exhibit*, 2002.

[5] Jörg R. Riccius, Oskar J. Haidn, and Evgeny B. Zametaev. Influence of time dependent effects on the estimated life time of liquid rocket combustion chamber walls. In *40th AIAA/ASME/SAE/ASEE Joint Propulsion Conference and Exhibit*, 2004.

[6] Jörg R. Riccius, Evgeny B. Zametaev, Oskar J. Haidn, and Gaelle de Boisvilliers. Comparison of 2d and 3d structural fe-analyses of lre combustion chamber walls. In *42th AIAA/ASME/SAE/ASEE Joint Propulsion Conference*, 2006.

[7] Jörg R. Riccius, Evgeny B. Zametaev, Oskar J. Haidn, and Christian Gogu. Lre chamber wall optimization using plane strain and generalized plane strain models. In *42nd AIAA/ASME/SAE/ASEE Joint Propulsion Conference and Exhibit*, 2006.

[8] W. Schwarz, S. Schwub, K. Quering, D. Wiedmann, H. W. Höppel, and M. Göken. Life prediction of thermally highly loaded components: Modelling of the damage process of a rocket combustion chamber hot wall. In *2010 Space Propulsion Conference*, 2010.

[9] J. Lemaitre and R. Desmorat. *Engineering Damage Mechanics*. Springer-Verlag, Berlin Heidelberg, 2005.

[10] I. N. Vladimirov, M. P. Pietryga, and S. Reese. On the modeling of nonlinear kinematic hardening at finite strains with application to springback - comparison of time integration algorithms. *International Journal of Numerical Methods in Engineering*, **75**:1–28, 2008.

[11] John J. Esposito and Ronald F. Zabora Thrust Chamber Life Prediction Volume I - Mechanical and Physical Properties of High Performance Rocket Nozzle Materials NASA Lewis Research Center, 1975.

[12] D. Kuhl and Jörg Riccius and O.J. Haidn Thermomechanical Analysis and Optimization of Cryogenic Liquid Rocket Engines *Journal of Propulsion and Power*, **18**:835–846, 2002.

[13] Ned P. Hannum and Harold G. Price, Jr. Some Effects of Thermal-Cycle-Induced Deformation in Rocket Thrust Chambers NASA Langley Research Center, 1981.